

Real-time evolution of a large-scale relativistic jet

Josep Martí^{1,5}, Pedro L. Luque-Escamilla^{2,5}, Gustavo E. Romero^{3,4,5}, Juan R. Sánchez-Sutil⁵, and Álvaro J. Muñoz-Arjonilla⁵

¹ Dept. de Física, EPS de Jaén, Universidad de Jaén, Campus Las Lagunillas s/n, A3-402, 23071 Jaén, Spain
e-mail: jmarti@ujaen.es

² Dept. de Ingeniería Mecánica y Minera, EPS de Jaén, Universidad de Jaén, Campus Las Lagunillas s/n, A3-402, 23071 Jaén, Spain
e-mail: peter@ujaen.es

³ Instituto Argentino de Radioastronomía, C.C.5, 1894 Villa Elisa, Buenos Aires, Argentina

⁴ Facultad de Ciencias Astronómicas y Geofísicas, Universidad Nacional de La Plata, Paseo del Bosque S/N, 1900, La Plata, Argentina
e-mail: gustavo.esteban.romero@gmail.com

⁵ Grupo de Investigación FQM-322, Universidad de Jaén, Campus Las Lagunillas s/n, A3-065, 23071 Jaén, Spain
e-mail: jrssutil@ujaen.es, ajmunoz@ujaen.es

Received xxxx, 2015; accepted xxxx, xxxx

ABSTRACT

Context. Astrophysical jets are ubiquitous in the Universe on all scales, but their large-scale dynamics and evolution in time are hard to observe since they usually develop at a very slow pace.

Aims. We aim to obtain the first observational proof of the expected large-scale evolution and interaction with the environment in an astrophysical jet. Only jets from microquasars offer a chance to witness the real-time, full-jet evolution within a human lifetime, since they combine a ‘short’, few parsec length with relativistic velocities.

Methods. The methodology of this work is based on a systematic recalibration of interferometric radio observations of microquasars available in public archives. In particular, radio observations of the microquasar GRS 1758–258 over less than two decades have provided the most striking results.

Results. Significant morphological variations in the extended jet structure of GRS 1758–258 are reported here that were previously missed. Its northern radio lobe underwent a major morphological variation that rendered the hotspot undetectable in 2001 and reappeared again in the following years. The reported changes confirm the Galactic nature of the source. We tentatively interpret them in terms of the growth of instabilities in the jet flow. There is also evidence of surrounding cocoon. These results can provide a testbed for models accounting for the evolution of jets and their interaction with the environment.

Key words. Stars: jets – ISM: jets and outflows – X-rays: binaries – Galaxies: jets – Stars: individual: GRS 1758–258

1. Introduction

Astrophysical jets are observed in a variety of environments (de Gouveia Dal Pino 2005) including young stellar and Herbig-Haro (HH) objects (Reipurth & Bally 2001), planetary nebulae (Sahai & Trauger 1998), microquasars (Mirabel & Rodríguez 1999), active galactic nuclei (AGN), and distant quasars (Begelman et al. 1984). These outflows are triggered when the magnetic field taps the rotational energy from a central compact object or disk (Blandford & Payne 1982; Kylafis et al. 2015). This mechanism is characterized well because the mass accretion and ejection events evolve fast enough to be appropriately sampled with multi-wavelength observations of both microquasars (Mirabel et al. 1998; Mirabel & Rodríguez 1994a; Fender et al. 1999) and AGN (Gómez et al. 2000; Marscher et al. 2002), where these processes occur on time scales from hours or days to years, respectively. However, the long-term evolution of the jet flow far away from the central engine is not understood as well. The large sizes of relativistic jets in AGN make them evolve on characteristic times of $\sim 10^6$ yr (Shabala et al. 2008), while the low velocities of HH jets imply shorter characteristic times of $\sim 10^3$ yr (de Gouveia Dal Pino

2001). Extended jets in both types of systems will then appear almost frozen during a human lifetime.

In this context, only microquasar jets that combine relatively short lengths and relativistic velocities (Mirabel & Rodríguez 1999) offer a chance to study large-scale jet dynamics and its interaction with the environment in almost real time. Here, we have paid attention to GRS 1758–258 which is believed to be a microquasar associated with a low-mass X-ray binary system. Although its Galactic nature has never been confirmed because of the lack of optical and infrared spectra of the companion star (Luque-Escamilla et al. 2014), GRS 1758–258 appears as a very bright and persistent hard X-ray source towards the Galactic centre region (Sunyaev et al. 1991). This source has strong spectral similarities in X-rays with the classical black hole candidate Cygnus X-1 (Main et al. 1999). It displays double-sided radio jets (Rodríguez et al. 1992; Mirabel & Rodríguez 1994b) whose arc-minute extension implies a parsec-scale linear size if located at the distance of the Galactic centre, hereafter assumed to be 8.5 kpc. In this Letter, we revisit the huge archive of GRS 1758–258 observations at radio wavelengths obtained with the Very Large Array (VLA) interferometer of the National Radio Astronomy Observatory (NRAO). This provides us with a unique set of highly sensitive maps with an angular resolu-

tion that is well suited to exploring the evolution of the GRS 1758–258 jets over more than a decade.

2. Data analysis and results

We data-mined the public archives of the VLA interferometer hosted by NRAO. The angular size and morphology of the arcminute GRS 1758–258 jets are well sampled by using the 6 cm wavelength and the C-configuration of the array. Two intermediate frequency bands 50 MHz wide were available from the VLA correlator products. A total of four useful observing projects between 1992 and 2008 could be retrieved with this instrumental setup (see first block of Table 1).

All downloaded projects were individually recalibrated by using the AIPS software package of NRAO, taking special care to remove corrupt visibilities in both the target and the calibrator sources. The phase calibrator was J1751–253, while the visibility amplitude was tied to the known flux densities of 3C286 and 3C48. Some older projects needed to be transformed from the B1950.0 to the J2000.0 reference system, by using the AIPS task UVFIX, in order to make the multi-epoch map comparison easier. Radio maps were created and deconvolved using the CLEAN algorithm as provided within the IMAGR task of AIPS. Their respective synthesized beams were individually determined first and later averaged. The resulting averaged elliptical Gaussian beam was finally used to convolve the clean components of each observing epoch in a second run of the IMAGR task.

In Fig. 1, we present the final sequence of 6 cm maps showing the appearance of the GRS 1758–258 during the years 1992, 1997, 2001, and 2008 on arcminute scales. The different panels can be considered as approximate matching-beam maps with similar point spread functions. Having the same angular resolution, they are therefore suitable for meaningful comparison of the jet morphological variations visible in different epochs. In all cases, natural weighting of the interferometric visibilities (i.e. a +5 value of the IMAGR ROBUST parameter) was applied to maximize sensitivity to extended emission. The AIPS task DBCON was used to concatenate short time slots of different VLA monitoring projects into a single observing epoch.

In Table 2 we compile the positions, deconvolved angular sizes, flux densities coming from the northern hotspot component that dominates the lobe emission, and its radio luminosities in the 0.1–10⁵ GHz range, assuming a –0.7 typical spectral index for non-thermal radio emission. We additionally include the minimum energy content and magnetic field assuming equipartition of energy between relativistic particles and magnetic field, using the Pacholczyk (1970) formulation. An estimate of the relativistic electron density needed to account for the observed radio luminosity is also given.

Finally, a few additional archive projects exist in the C, D and CD configurations (see 2nd block of Table 1). Although there was not high enough quality to provide new individual frames in Fig. 1, they were selected to enhance the sensitivity to extended emission in deep imaging that is discussed below.

3. Discussion

In 1992, the jet’s northern lobe in Fig. 1 ended in a sort of bow-shaped working surface with a conspicuous component at its vertex that we interpret as the terminal hotspot. Comparison with the 1997 frame, where the hotspot is brighter and easily recognized, implies a noticeable shift of $13'' \pm 1''$ on a time interval of 5.4 yr. This value is consistent with previous, very conservative upper limits that supported the idea of a continuously

Table 1. Log of VLA 6 cm observations used in this work.

Project code	VLA config.	Observation date	On-source time (s)	Central Julian day
AM345	C	1992 Mar 21	1770	
		1992 Apr 09	6040	2448719
AM560	C	1992 Apr 11	2610	
		1997 Aug 03	2440	
		1997 Aug 05	2440	
		1997 Aug 08	2440	
		1997 Aug 11	2160	
		1997 Aug 14	2170	2450674
		1997 Aug 15	1860	
		1997 Aug 18	2450	
AR458	C	1997 Aug 20	2430	
		1997 Aug 24	2420	
		2001 Jul 08	473	
		2001 Jul 24	533	
		2001 Aug 4	673	
		2001 Aug 9	603	
		2001 Aug 16	453	2452132
		2001 Aug 26	413	
AS930	C	2001 Aug 30	403	
		2001 Sep 07	533	
		2008 Apr 01	4840	
		2008 Apr 07	4840	2454563
		2008 Apr 12	4840	
AM345	D	1992 Sep 26-27	5690	2448892
AM428	CD	1993 Oct 3-4	6460	2448899
AR476	C	2002 Oct 15	1453	
		2002 Oct 16	1513	2452582
		2002 Nov 11	1623	
		2002 Dec 2	1533	
AR523	C	2004 Apr 30	953	2453126
		2004 May 05	953	2453131

powered stationary jet flow (Martí et al. 2002; Soria et al. 2011). When assuming the hotspot identification is correct, the $2''.4 \pm 0''.2 \text{ yr}^{-1}$ associated proper motion translates into a velocity of the projected jet head of $(0.32 \pm 0.03)c$, where c is the speed of light. In the 2001 frame, the northern jet lobe was observed to evolve into two elongated fragments that were nearly parallel to the jet direction. The conspicuous hotspot of 1997 completely lost its shape, and only traces of its extended emission remained at its position after four years. Seven years later, in 2008, a new hotspot had clearly reappeared at some time in between. Had the 2008 northern hotspot existed in 2001, it should have been detected well above the rms noise. Moreover, from Table 2 the position offset between the 1997 and 2008 hotspots is estimated to be $1''.9 \pm 0''.7$. Thus, we are observing a newly formed structure. On the other hand, the southern counter-jet is also visible in Fig. 1, but it did not display a structure that was as well organized as the northern jet. Only hints of precession previously noticed by Martí et al. (2002) are evident in 1997, but they are remarkably absent in the even more sensitive 2008 frame. This is additional evidence that the GRS 1758–258 jet evolution is real.

The low declination of the source limits the achievable dynamic ranges of the Fig. 1 maps. Therefore, difference maps were computed to assess the reliability of the observed structural variations better. Our two more sensitive observing epochs were used for this purpose. Figure 2 shows a zoomed view of morphology differences in the northern hotspot, together with the subtraction of the 1997 clean component model from the 2008

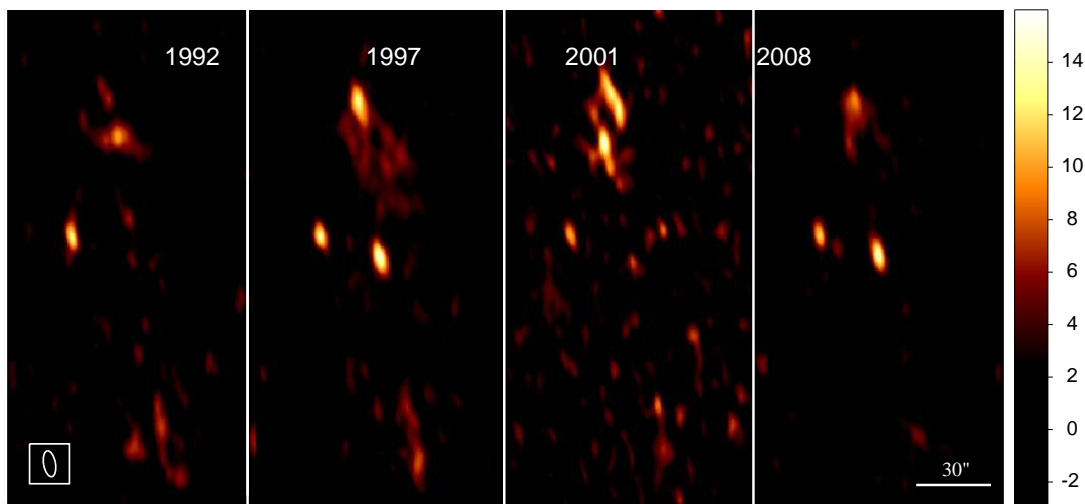


Fig. 1. Time evolution of the GRS 1758–258 extended radio jets as observed with the VLA interferometer at the 6 cm wavelength (4.8 GHz) over sixteen years (1992–2008) with nearly identical angular resolution. North is up and east to the left. The horizontal bar at the bottom right corner shows the angular scale. The interferometric synthesized beam is $10''.50 \times 4''.75$, with position angle of 10° (bottom left ellipse). The vertical colour bar provides a linear brightness scale in units of $\mu\text{Jy beam}^{-1}$. The rms background noise is 10, 10, 19 and $8 \mu\text{Jy beam}^{-1}$ for the 1992 to 2008 frames, respectively. The two variable point sources are the GRS 1758–258 central core and an unrelated object about $25''$ to the east of it.

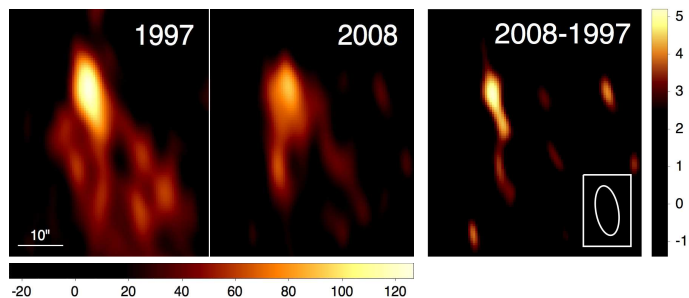


Fig. 2. Close up of the northern radio lobe of GRS 1758–258 as observed with the VLA at 6 cm in 1997 (left) and 2008 (middle), when the hotspot was fainter. The coloured horizontal bar provides a linear intensity scale in $\mu\text{Jy beam}^{-1}$. The bottom left corner bar gives the angular scale. North is up and east left. The right panel shows the residual difference between the two epochs. Its colour vertical bar is scaled in units of the rms noise in the difference map ($10 \mu\text{Jy beam}^{-1}$). The synthesized beam in all panels is the same as in Fig. 1 (bottom right ellipse).

visibility data. Residuals emerge at the 4σ to 5σ level. Beyond the field of view shown here, they are also aligned along the jet position angle, suggesting changes that affect the whole jet flow.

The first consequence of the observed phenomena is an upper limit to the GRS 1758–258 distance. This comes from the time scale ($\tau \sim 11$ yr) of major structural changes. The northern jet flow was fully renewed between 1997 and 2008, as shown in Figs. 1, and 2. Given its angular size ($\theta \sim 60''$), causality arguments dictate that the maximum possible distance lies within the boundaries of the Milky Way ($\sim c\tau/\theta \sim 12$ kpc). Having the jet inclined with respect to the line-of-sight would reduce this value further. Therefore, the Galactic origin of GRS 1758–258 becomes fully confirmed for the first time.

The physical interpretation of these morphological changes is uncertain, although their disruptive appearance suggests that they may be due to the onset of hydrodynamic instabilities (Birkinshaw 1997) such as Kelvin-Helmholtz (KH) or Rayleigh-Taylor (RT) instabilities. The stability condition essentially depends on the ratio $\eta = n_j/n_a$ with n_j and n_a the density of the

jet and the ambient medium, respectively. If $\eta < 1$, the jet may be unstable. When assuming that GRS 1758–258 jet is baryonic and that most of the mass flux is in the form of a thermal plasma (e.g., about 90%), the relativistic particles responsible for the non-thermal radio emission, whose density of $\sim 10^{-3} \text{ cm}^{-3}$ has been estimated from equipartition (see Table 2), account for the remaining 10%. Thus, the actual jet density is tentatively estimated as $n_j \sim 10^{-2} \text{ cm}^{-3}$.

Given that microquasars are typically located in much less dense environments than the canonical interstellar medium (Heinz 2002), we assume $n_a \sim 0.1 \text{ cm}^{-3}$. This yields a density contrast in the vicinity of the terminal hotspot of $\eta \sim 10^{-1}$. Therefore, the jet could be prone to undergoing hydrodynamic instabilities, and its disruption may occur if the KH or RT modes have enough time to grow up to a length scale comparable to the jet radius r_j . These time scales may be calculated (Araudo et al. 2009, 2010) as $t_{KH} \sim (2r_j/c)\eta^{1/2}$ and $t_{RT} \sim (2r_j/c)(2\eta/3)^{1/2}$, respectively. When assuming that the filaments of radio emission converging to the hotspot in Fig. 2 are actually tracing the jet flow, $r_j \sim 0.1$ pc for GRS 1758–258 at its estimated distance. Taking this value, growth time scales of destructive RT and KH instabilities are found to be very similar and to last several months.

Considering the uncertainties involved in this calculation, it thus appears conceivable from the physical point of view that the GRS 1758–258 jets undergo RT and/or KH instabilities that completely reorganize their collimated outflow on a yearly time scale, as suggested by the multi-epoch observations reported in this work. In the maps presented in Fig. 1, we have merged data sets scattered over no more than a two-months span, so that they are safely below the limit for avoiding an excessive smearing of the imaged structures.

We emphasize that changes in the microquasar central engine cannot be responsible for the morphological disruption of the outer jet, since the cooling time t_c of relativistic electrons by synchrotron radiation in the jet head is too long. Specifically, $t_c[\text{s}] \sim 5 \times 10^8 \gamma^{-1} B^{-2}$, where γ is the Lorentz factor of the electrons and B the magnetic field in Gauss. For $B \sim 10^{-5}$ G and $\gamma \sim 10^6$, we get $t_c \sim 3$ Myr! It is clear that the struc-

Table 2. Observational parameters for the northern hotspot of GRS 1758–258 at the 6 cm wavelength

Epoch	R. A. (J2000.0) 18^h01^m	Dec. (J2000.0) $-25^\circ43'$	Flux density (mJy)	Deconvolved angular size (arc-second ²)	Radio luminosity (erg s ⁻¹)	Minimum energy (erg)	Magnetic field (Gauss)	Relativistic e- density (cm ⁻³)
1992	$12^s8 \pm 0^s1$	$48'' \pm 1''$	0.37 ± 0.03	$(18 \pm 3) \times (\leq 9)$	1.0×10^{31}	$\leq 3.3 \times 10^{44}$	$\geq 4.0 \times 10^{-5}$	$\geq 7.6 \times 10^{-4}$
1997	$13^s00 \pm 0^s02$	$35''6 \pm 0''7$	0.26 ± 0.02	$(15 \pm 2) \times (6 \pm 1)$	7.1×10^{30}	1.9×10^{44}	4.7×10^{-5}	1.0×10^{-3}
2001 ^a	$12^s9 \pm 0^s1$ $13^s13 \pm 0^s03$	$33'' \pm 1''$ $52'' \pm 1''$	0.29 ± 0.04 0.26 ± 0.04	$(25 \pm 4) \times (4 \pm 2)$ $(24 \pm 6) \times (3 \pm 2)$	7.9×10^{30} 7.1×10^{30}	2.1×10^{44} 1.6×10^{44}	4.6×10^{-5} 5.1×10^{-5}	1.2×10^{-3} 1.1×10^{-3}
2008	$13^s11s \pm 0^s03$	$36''8 \pm 0''6$	0.18 ± 0.02	$(13 \pm 2) \times (8 \pm 1)$	4.9×10^{30}	1.6×10^{44}	3.9×10^{-5}	7.4×10^{-4}

^(a) Northern hotspot appears to have fragmented into two components. Data for both are given.

ture must be destroyed and the electrons then diffuse into the interstellar medium, escaping from the region where they were confined. This plasma leaving the hotspot can form a cocoon structure around the radio lobes, creating cavities or bubbles, as seen in the environment of Galactic and extragalactic sources of relativistic jets with continued activity (Kawakatu & Kino 2006; Gallo et al. 2005; Wilson et al. 2006; Pakull et al. 2010). In this context, it makes sense to wonder if this cocoon structure also exists in GRS 1758–258. To shed light on this issue, we decided to concatenate all observational projects in Table 1 to produce the deepest radio map available for this microquasar (see Fig. 3). The total on-source integration time of this huge data set amounts to about 19^h , allowing us to reach a background rms noise of $6 \mu\text{Jy beam}^{-1}$ with natural weight. In this map, bridges of extended emission emanate from both radio lobes and almost surround the whole bipolar jet complex with an elliptical shape. The faintest cocoon edges appear at a 4σ level and cover more than 50% of the elliptical perimeter. Such diffuse features reveal, for the first time, the expected cocoon-like structure around GRS 1758–258. This is a new similarity between microquasars and radio galaxies that has never been observed before.

New, more sensitive multi-wavelength observations will provide a benchmark for validating our current ideas of the processes involving collimated flows in astrophysical contexts, which otherwise could not be appropriately sampled in time. For instance, detailed changes in jet structures and fainter cocoon shells created by jet relict particles should be revealed by new radio interferometers, such as EVLA, LOFAR, or SKA.

Acknowledgements. This work was supported by grant AYA2013-47447-C3-3-P from the Spanish Ministerio de Economía y Competitividad (MINECO), and by the Consejería de Economía, Innovación, Ciencia y Empleo of Junta de Andalucía under excellence grant FQM-1343 and research group FQM-322, as well as FEDER funds. GER is a member of CONICET. The National Radio Astronomy Observatory is a facility of the National Science Foundation operated under cooperative agreement by Associated Universities, Inc.

References

- Araudo, A. T., Bosch-Ramon, V., & Romero, G. E. 2009, *A&A*, 503, 673
Araudo, A. T., Bosch-Ramon, V., & Romero, G. E. 2010, *International Journal of Modern Physics D*, 19, 931
Begelman, M. C., Blandford, R. D., & Rees, M. J. 1984, *Reviews of Modern Physics*, 56, 255
Birkinshaw, M. 1997, in *Advanced Topics on Astrophysical and Space Plasmas*, eds. E.M. Gouveia Dal Pino, A.L. Peratt, G.A. Medina Tancro, A.C.-L. Chian; Kluwer: Dordrecht, 17, 17
Blandford, R. D. & Payne, D. G. 1982, *MNRAS*, 199, 883
de Gouveia Dal Pino, E. M. 2001, *ApJ*, 551, 347
de Gouveia Dal Pino, E. M. 2005, *Advances in Space Research*, 35, 908
Fender, R. P., Garrington, S. T., McKay, D. J., et al. 1999, *MNRAS*, 304, 865
Gallo, E., Fender, R., Kaiser, C., et al. 2005, *Nature*, 436, 819
Gómez, J.-L., Marscher, A. P., Alberdi, A., Jorstad, S. G., & García-Miró, C. 2000, *Science*, 289, 2317

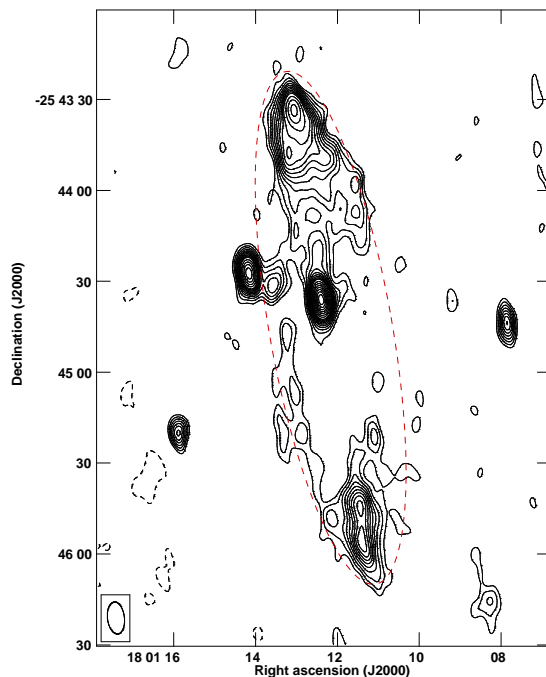


Fig. 3. Natural-weight 6 cm map of GRS 1758–258 and its surrounding cocoon diffuse emission obtained by combining all VLA data sets (see Table 1). The horizontal bar in the top right corner gives the angular scale. The dashed red ellipse sketches the edges of a previously unseen, cocoon-like structure around this microquasar. The synthesized beam of $10''.6 \times 5''.6$, with position angle $6^\circ.7$, is displayed by the bottom left ellipse. Contours shown correspond to $-3, 3, 4, 5, 6, 7, 8, 9, 10, 11, 12, 14, 16, 18, 20, 22, 24$, and 26 times the rms background noise of $6 \mu\text{Jy beam}^{-1}$. Three unrelated compact radio sources also appear in this map.

- Heinz, S. 2002, *A&A*, 388, L40
Kawakatu, N. & Kino, M. 2006, *MNRAS*, 370, 1513
Kylafis, N., Gabuzda, D., & Contopoulos, I. 2015, *The Formation and Disruption of Black Hole Jets*, *Astrophysics and Space Science Library* (Springer)
Luque-Escamilla, P. L., Martí, J., & Muñoz-Arjonilla, Á. J. 2014, *ApJ*, 797, L1
Main, D. S., Smith, D. M., Heindl, W. A., et al. 1999, *ApJ*, 525, 901
Marscher, A. P., Jorstad, S. G., Gómez, J.-L., et al. 2002, *Nature*, 417, 625
Martí, J., Mirabel, I. F., Rodríguez, L. F., & Smith, I. A. 2002, *A&A*, 386, 571
Mirabel, I. F., Dhawan, V., Chaty, S., et al. 1998, *A&A*, 330, L9
Mirabel, I. F. & Rodríguez, L. F. 1994a, *Nature*, 371, 46
Mirabel, I. F. & Rodríguez, L. F. 1994b, in *American Institute of Physics Conference Series*, Vol. 304, *American Institute of Physics Conference Series*, ed. C. E. Fichtel, N. Gehrels, & J. P. Norris, 413–420
Mirabel, I. F. & Rodríguez, L. F. 1999, *ARA&A*, 37, 409
Pacholczyk, A. 1970, *Radio Astrophysics: Nonthermal Processes in Galactic and Extragalactic Sources*, *Astronomy and Astrophysics Series* (W. H. Freeman)
Pakull, M. W., Soria, R., & Motch, C. 2010, *Nature*, 466, 209
Reipurth, B. & Bally, J. 2001, *ARA&A*, 39, 403

- Rodríguez, L. F., Mirabel, I. F., & Martí, J. 1992, *ApJ*, 401, L15
Sahai, R. & Trauger, J. T. 1998, *AJ*, 116, 1357
Shabala, S. S., Ash, S., Alexander, P., & Riley, J. M. 2008, *MNRAS*, 388, 625
Soria, R., Broderick, J. W., Hao, J., et al. 2011, *MNRAS*, 415, 410
Sunyaev, R., Churazov, E., Gilfanov, M., et al. 1991, *A&A*, 247, L29
Wilson, A. S., Smith, D. A., & Young, A. J. 2006, *ApJ*, 644, L9